

# Simultaneous whole-animal 3D-imaging of neuronal activity using light field microscopy

Robert Prevedel<sup>1-3,\*</sup>, Young-Gyu Yoon<sup>4,5,\*</sup>, Maximilian Hoffmann<sup>1-3</sup>, Nikita Pak<sup>5,6</sup>, Gordon Wetzstein<sup>5</sup>, Saul Kato<sup>1</sup>, Tina Schrödel<sup>1</sup>, Ramesh Raskar<sup>5</sup>, Manuel Zimmer<sup>1</sup>, Edward S. Boyden<sup>5,7,8</sup>, Alipasha Vaziri<sup>1-3</sup>

<sup>1</sup>Research Institute of Molecular Pathology, Vienna, Austria.

<sup>2</sup>Max F. Perutz Laboratories, University of Vienna, Vienna, Austria.

<sup>3</sup>Research Platform Quantum Phenomena & Nanoscale Biological Systems (QuNaBioS), University of Vienna, Vienna, Austria.

<sup>4</sup>Department of Electrical Engineering and Computer Science, Massachusetts Institute of Technology (MIT), Cambridge, MA, USA

<sup>5</sup>MIT Media Lab, Massachusetts Institute of Technology (MIT), Cambridge, MA, USA

<sup>6</sup>Department of Mechanical Engineering, Massachusetts Institute of Technology (MIT), Cambridge, MA, USA

<sup>7</sup>Departments of Biological Engineering and Brain and Cognitive Sciences, Massachusetts Institute of Technology (MIT), Cambridge, MA, USA

<sup>8</sup>McGovern Institute, Massachusetts Institute of Technology (MIT), Cambridge, MA, USA

\* These authors contributed equally to this work.

Correspondence should be addressed to E.S.B. (esb@media.mit.edu) or A.V. (vaziri@imp.ac.at).

**3D functional imaging of neuronal activity in entire organisms at single cell level and physiologically relevant time scales faces major obstacles due to trade-offs between the size of the imaged volumes, and spatial and temporal resolution. Here, using light-field microscopy in combination with 3D deconvolution, we demonstrate intrinsically simultaneous volumetric functional imaging of neuronal population activity at single neuron resolution for an entire organism, the nematode *Caenorhabditis elegans*. The simplicity of our technique and possibility of the integration into epi-fluorescence microscopes makes it an attractive tool for high-speed volumetric calcium imaging.**

In order to understand how sensory inputs are dynamically mapped onto functional activity of neuronal populations and how their processing leads to cognitive functions and behavior, tools for non-invasive interrogation of neuronal circuits with high spatio-temporal resolution are required <sup>1,2,3</sup>. Recent efforts have led to a number of approaches for 3D neural activity imaging, taking advantage of exciting chemical and genetically encoded fluorescent reporters <sup>4,5,6</sup>. While some are based on scanning the excitation light to different points in a volume, either sequentially <sup>7,8,9,10,11</sup> or randomly <sup>12,13,14,15</sup>, others try to capture 3D image data simultaneously by mapping axial information onto a single lateral plane for acquisition by a camera using multifocal imaging <sup>16,17</sup>, aperture coding

18,19,20,21, stereoscopic vision<sup>22</sup>, light-fields<sup>23,24,25,26</sup> or other approaches<sup>27,28,29,30</sup>. The former methods are inherently limited by the time that it takes to scan a desired volume, whereas the latter methods face other types of tradeoffs such as between spatial resolutions and the size of the imaged volume.

Light-field microscopy (LFM)<sup>25</sup> is one of such methods. It has been successfully applied to imaging still and *in-vitro* biological samples<sup>25,26</sup>, and also to control light illumination in microscopy<sup>26,27</sup>. However, to date, despite its superb temporal resolution, LFM has not been used for any functional biological imaging. This is because of its reduced spatial resolution compared to standard scanning methods and the inherent trade-off between the spatial and axial resolution as well as axial imaging range<sup>25</sup>.

Here, we report that neural systems equipped with calcium sensors can be imaged at volume rates up to 50Hz and with single neuron resolution, using a 3D deconvolution algorithm<sup>31,32</sup> applied to LFM. We achieve an effective resolution of  $\sim 1.4\mu\text{m}$  and  $2.6\mu\text{m}$  in the lateral and axial dimensions respectively, inside biological samples, and demonstrate simultaneous recording of neuronal population activity over a field of view of  $\sim 350\mu\text{m} \times 350\mu\text{m} \times 30\mu\text{m}$ . This is sufficient to capture the dynamics of neurons distributed across the entire nervous system of *Caenorhabditis elegans*. In particular, we show that the activity of the majority of head ganglia neurons together with selected neurons from the ventral cord can be recorded simultaneously. Our light field deconvolution setup can be easily integrated into most commercial epi-fluorescence microscopes and provides a simple and cost-effective addition to these platforms.

A microscope can be converted to a LFM by placing a microlens array at its intermediate image plane (Figure 1a and Methods). The camera sensor behind these microlenses captures different perspectives of the sample from several viewing angles (Figure 1b). The product of angular information, which effectively underlies the axial resolution, and the spatial, orthographic information, is recorded on the image sensor. This leads to an intrinsic trade-off between axial and lateral spatial resolution in LFM that results in a decrease of the latter in most practical situations compared to a standard microscope. However, by exploiting aliasing of the recorded data, computational reconstruction methods based on 3D-deconvolution can effectively reconstruct volumes with improved spatial resolution<sup>31,32</sup> (see Methods and Supplementary Notes for details).

To evaluate the spatial resolution of our light field deconvolution microscope (LFDM) we image sub-diffraction beads and then reconstruct the point-spread function (PSF) of our system (Figure 1b-c). Using LFDM, we find a resolution of  $\sim 1.4\mu\text{m}$  ( $2.6\mu\text{m}$ ) in the lateral (axial) dimension. To further verify the suitability of LFDM for capturing the activity of individual neurons in *C. elegans*, we image a sample consisting of  $6\mu\text{m}$ -sized fluorescent beads that are randomly distributed in all three dimensions and suspended in agarose. We then directly compare a high resolution, conventional focal stack (taken without microlenses) of this sample (Figure 1d-e) with the deconvolved light-field images from the same beads (Figure 1f-g). The ability to resolve these randomly distributed and evenly fluorescing beads shows that our light-field microscope should also resolve individual neurons in the densely packed head ganglia region of *C. elegans*. In worms the unambiguous segmentation of individual neurons is additionally

facilitated by the nuclear confinement of the nls-GCaMP5K Ca<sup>2+</sup>-reporter and by exploiting the modulation of fluorescence emission during neuronal activity. This represents a major advantage of our approach as it alleviates the need to additionally employ more complex signal detection and unmixing methods which otherwise would be necessary to obtain single-neuron resolution<sup>33,34</sup>.

In functional imaging experiments of *C. elegans*, we record data over the entire area of our camera sensor, resulting in a field-of-view that spans ~350 μm x 350 μm x 30 μm. We can thus image the majority of the worm while maintaining single-neuron resolution (Fig. 2a-c; Supplementary Figure S1 and Supplementary Video 1 - 2). We are able to image the activity of neurons in the brain region surrounding the nerve ring as well as along the ventral cord with sufficient temporal resolution (5Hz). We note that significantly higher volume acquisition speed would be possible given the maximum frame rate of our camera and we demonstrate this by capturing the activity of head ganglia neurons at 50Hz volume rate (see Supplementary Video 3). Such volume rates would be in principle sufficient for future studies involving whole brain imaging of freely moving worms<sup>35</sup>. However, since Ca<sup>2+</sup>-signals in *C. elegans* occur at timescales of up to 1 Hz only, we have chosen longer exposure times and hence slower volume rates of 5Hz in order to benefit from faster time-series reconstruction and to maximize GCaMP signal-to-noise while preventing potential photo-bleaching during recordings. The wide field of view of LFDM and the intrinsic simultaneity of the acquisition allow studying correlation between far-away neurons, which would not be accessible with other Ca<sup>2+</sup>-imaging techniques such as multifocal imaging<sup>16,17</sup>, which also features simultaneous volume acquisition, but of only ~10-50 times smaller volumes. In our experiments, we observe correlated and anti-correlated activity patterns between the head-ganglia neurons and motor neurons located along the ventral side of the worm, which connect to body wall muscles and are responsible for generating undulatory locomotion (see Fig. 2a-c).

We have also performed experiments in which we record exclusively from brain regions surrounding the nerve ring (Fig. 2d-f, and Supplementary Fig. S1). Imaging smaller field of views (~200x70x30μm) leads to faster volume reconstruction and less artifacts stemming from brightly fluorescent cells, such as coelomocytes. In a typical recording, we are able to resolve up to 74 individual neurons, of which around 30 show pronounced activity over the recording time of 200 seconds (Fig. 2d-f, and Supplementary Fig. S2). These results are comparable to that obtained with other recent demonstrations in whole-brain Ca<sup>2+</sup>-imaging experiments in *C. elegans*<sup>8</sup>.

In summary, we have implemented a LFM system and discovered its ability to allow simultaneous volumetric imaging of neuronal population activity at single cell resolution for the entire nervous system of *C. elegans*. This is achieved by light field deconvolution during post-processing which effectively increases the 3D volume resolution. Simultaneous acquisition of the entire volumes eliminates spatio-temporal ambiguity associated with sequentially recorded approaches and decouples temporal resolution from volume size. Resolution in all three dimensions are set by objective and microlens properties, while field of view and acquisition rate are determined by camera chip size and frame rates as well as signal intensity, respectively. LFDM is easy to set-up, cost-effective and

compatible with standard microscopes. In addition both the temporal resolution and the size of the field of views that can be imaged, make LFDM an attractive technique for future combination with behavioral studies, where representation and processing of information by an entire nervous system, from sensory input neurons to motor neurons could be investigated. Thus, we expect that this 3D imaging method will find rapid and widespread use within the neuroscience community. Future work will focus on scalability, faster and more efficient computational reconstruction techniques as well as applying the technique to neuronal networks of larger model organisms. Combining this approach with red-shifted Ca<sup>2+</sup>-sensors<sup>36,37,38</sup> as well as techniques such as adaptive optics<sup>39</sup> for aberration correction and imaging at depth in biological tissue<sup>40</sup> promises even more wide-spread applicability of LFDM.

## Methods

The LFM system is appended to an epi-fluorescence microscope (Zeiss, Axiovert 200) equipped with a LED excitation light source ( $\lambda=488\text{nm}$ , 300 mW, CoolLED, Andover) and a standard GFP filter set (Zeiss). For the high-speed imaging experiment displayed in Supplementary Video 3, a laser was coupled into the excitation pathway to increase the excitation power needed for the short exposure times ( $\lambda=488\text{nm}$ , 25mW, Coherent Inc.). In all imaging experiment, we use a 40x 0.95NA dry objective (Zeiss APOCHROMAT). The microlens array is mounted inside a 5-axis kinematic mount (Thorlabs) to allow fine adjustment of the array orthogonal to the optics axis, which we found crucial for high-quality results. The array is further imaged onto a 5.5 Megapixel (2560x2160 pixels) sCMOS camera (Andor Zyla) utilizing a 1:1 relay macro lens objective (Nikon AF-S 105mm 2.8 G VR IF-ED Micro) (see Fig. 1a). Details on optical design choices and their effect on resolution are discussed in Supplementary Note 1.

To record neuronal activity from *C. elegans*, we load adult worms (one- to four-egg-stage) expressing nls-GCaMP5k under the *punc31*-promoter into a microfluidic channel which is connected to a reservoir containing S-Basal buffer with 5 mM tetramisole, an acetylcholine receptor-specific agonist that mildly paralyzes the animal's muscles to reduce motion<sup>8</sup>. The worm is placed off the native focal plane and towards the objective using a piezo stepper motor (PI-721, Physik Instrumente GmbH), such that the entire worm is ideally contained in the region spanning  $-30\mu\text{m}$  to  $0\mu\text{m}$ . By doing so we exploit the highest resolution of LFDM while avoiding artifacts near the focal plane. When recording from the head region only, the worm's head ganglia are placed at the center of the field of view and excitation is limited to this area by the use of an iris in the excitation pathway. This ensures that brightly fluorescent cells outside the brain region are not excited and thus do not exacerbate the volume reconstruction.

The volume reconstruction itself can be formulated as a tomographic inverse problem<sup>41</sup>, where multiple different perspectives of an unknown 3D volume are observed, and linear reconstruction methods—implemented via deconvolution—are employed for computational 3D volume reconstruction. The image formation in light-field microscopes involves diffraction from both the objective and microlenses. Point spread functions for the deconvolution can be computed from vectorial diffraction theory<sup>42</sup>. More details are given in Supplementary Note 2.

After recording of the raw light field images, the digital images are cropped to regions of interest and resampled to contain 15x15 angular light field samples under each lenslet. Two calibration images, one showing the microlenses with collimated rear-illumination and one showing a uniform fluorescent slide, are used for digital image rectification, in which camera pixels are assigned to individual microlenses. Reconstruction of each frame of an image sequence takes between 3 and 20 minutes, depending on the size of the image, number of iterations of the deconvolution algorithm and workstation used. Computational resources are further discussed in Supplementary Note 2.

To extract a fluorescence time series for individual neurons from the raw video movies, we first applied rigid-body motion correction to each individual z plane movie. We then computed a median-intensity projection through time for each motion-corrected z plane movie and used a maxima-finding algorithm to identify areas of peaked intensity in each projection. A circular region of interest (ROI) was created surrounding each intensity peak, and overlapping ROI areas within Z planes were eliminated. ROIs in adjacent Z planes within an x-y distance of 7 pixels were considered to be a component of the same neuron, up to a maximum of 5 planes, and for each neuron at each time point, the brightest 100 pixels of the aggregate of all pixels within the neuron's component ROIs were averaged to produce a single fluorescence value. To extract  $\Delta F/F_0$ , we calculated  $\Delta F/F_0 = 100 * (F_{(t)} - F_0)/F_0$ , with  $F_0$  being the mean fluorescence intensity of each corrected trace.

## ACKNOWLEDGMENTS

We thank T. Müller, P. Pasierbek, H. Kaplan and M. Molodtsov for technical support and loan of equipment. R.P. acknowledges the VIPS Program of the Austrian Federal Ministry of Science and Research and the City of Vienna as well as the European Commission (Marie Curie, FP7-PEOPLE-2011-IIF). Y.-G.Y. acknowledges the support from Samsung Scholarship. The research leading to these results has received funding from the Vienna Science and Technology Fund (WWTF) project VRG10-11, Human Frontiers Science Program Project RGP0041/2012, Research Platform Quantum Phenomena and Nanoscale Biological Systems (QuNaBioS) and Research Institute of Molecular Pathology (IMP). M.Z. and T.S. received funding from the European Community's Seventh Framework Programme (FP7/2007-2013)/ERC grant agreement no. 281869 – *elegansNeurocircuits*. The IMP is funded by Boehringer Ingelheim.

## AUTHOR CONTRIBUTIONS

R.P. designed microlenses, built the initial imaging system and performed experiments together with M.H. Y.-G.Y. designed and wrote 3D-deconvolution software with contributions from G.W. under the guidance of R.R. R.P., Y.-G.Y. and M.H. analyzed data; N.P. implemented and tested LFDM prototype; T.S. and M.Z. designed and contributed NLS-GCaMP5K and the microfluidic device; K.S. wrote analysis software. E.S.B. and A.V. conceived and led project. R.P., Y.-G.Y. and A.V. wrote the manuscript, with input from all authors.

## COMPETING FINANCIAL INTERESTS

The authors declare no competing financial interests.

## REFERENCES

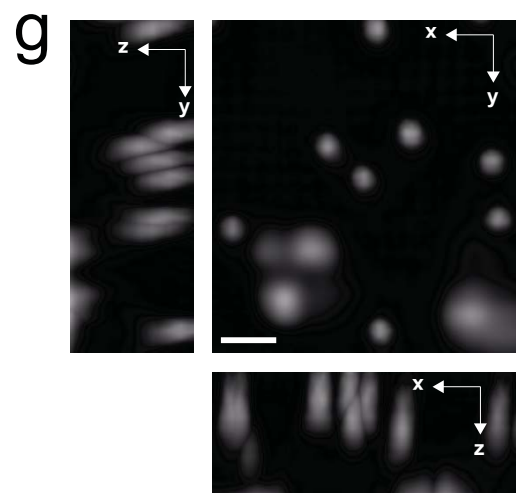
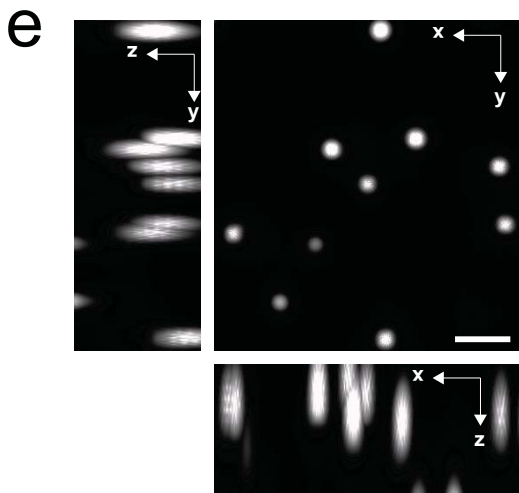
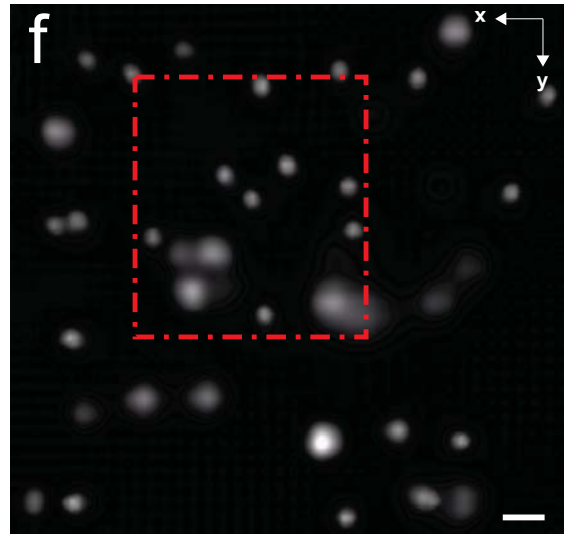
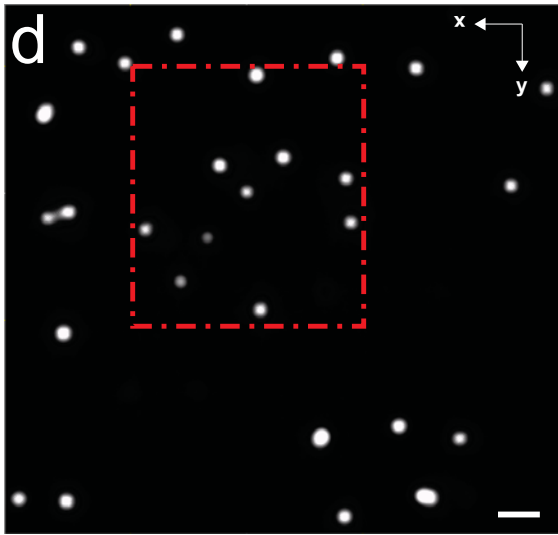
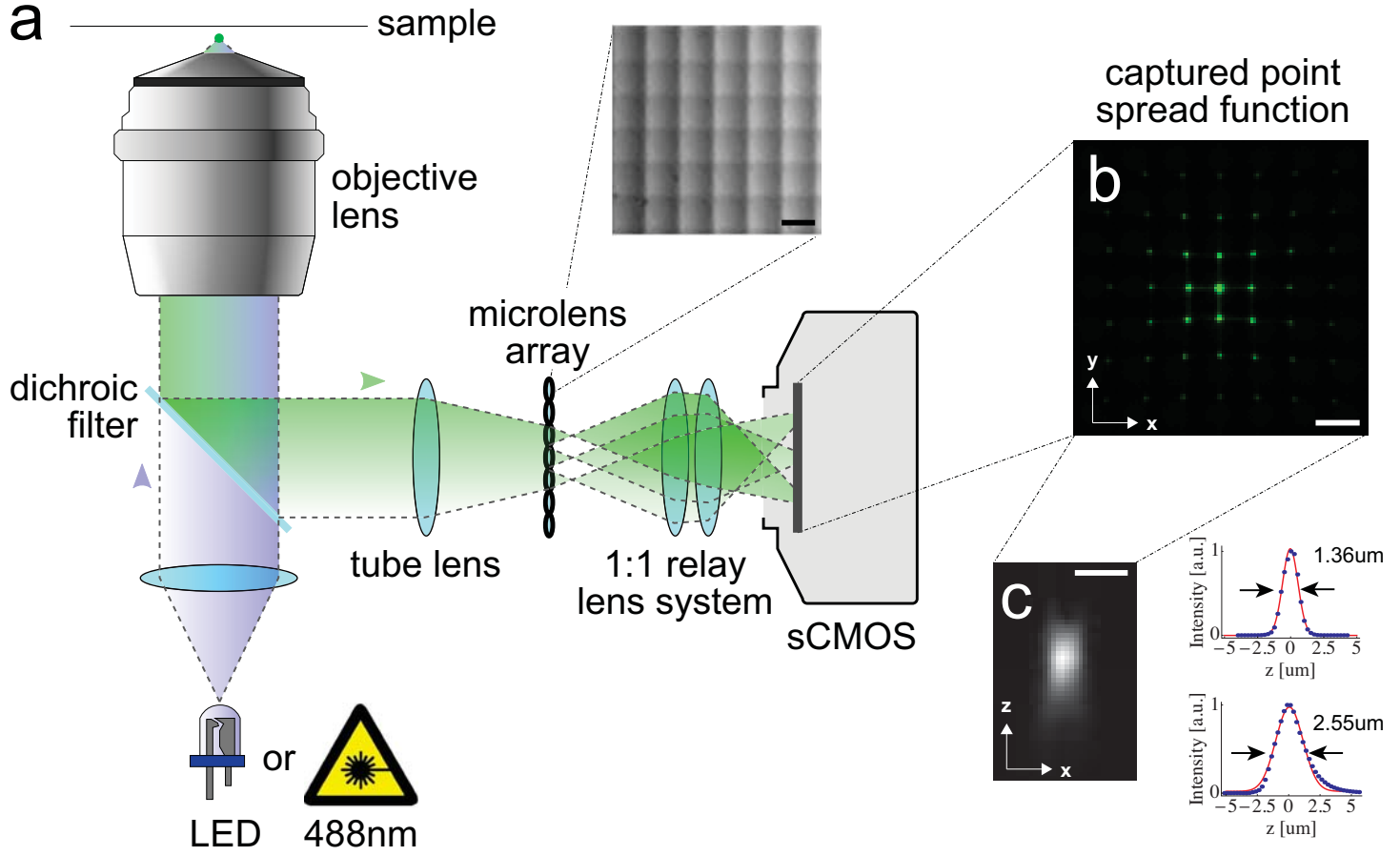
- 1 Alivisatos, A. P. *et al.* The Brain Activity Map Project and the Challenge of Functional Connectomics. *Neuron* **74**, 970-974, doi:10.1016/j.neuron.2012.06.006 (2012).
- 2 Bargmann, C. I. Beyond the connectome: How neuromodulators shape neural circuits. *Bioessays* **34**, 458-465, doi:10.1002/bies.201100185 (2012).
- 3 Marblestone, A. H. *et al.* Physical principles for scalable neural recording. *Front. Comput. Neurosci.* **7**, 34, doi:10.3389/fncom.2013.00137 (2013).
- 4 Stosiek, C., Garaschuk, O., Holthoff, K. & Konnerth, A. In vivo two-photon calcium imaging of neuronal networks. *Proc Natl Acad Sci U S A* **100**, 7319-7324, doi:10.1073/pnas.1232232100 1232232100 [pii] (2003).
- 5 Chen, T.-W. *et al.* Ultrasensitive fluorescent proteins for imaging neuronal activity. *Nature* **499**, 295-300 (2013).
- 6 Cao, G. *et al.* Genetically Targeted Optical Electrophysiology in Intact Neural Circuits. *Cell* **154**, 904-913, doi:10.1016/j.cell.2013.07.027 (2013).
- 7 Denk, W., Strickler, J. H. & Webb, W. W. Two-photon laser scanning fluorescence microscopy. *Science* **248**, 73-76 (1990).
- 8 Schrodell, T., Prevedel, R., Aumayr, K., Zimmer, M. & Vaziri, A. Brain-wide 3D imaging of neuronal activity in *Caenorhabditis elegans* with sculpted light. *Nature Methods* **10**, 1013-+, doi:10.1038/nmeth.2637 (2013).
- 9 Ahrens, M. B. & Keller, P. J. Whole-brain functional imaging at cellular resolution using light-sheet microscopy. *Nature methods*, doi:10.1038/nmeth.2434 (2013).
- 10 Panier, T. *et al.* Fast functional imaging of multiple brain regions in intact zebrafish larvae using Selective Plane Illumination Microscopy. *Frontiers in neural circuits* **7**, 65, doi:10.3389/fncir.2013.00065 (2013).
- 11 Turaga, D. & Holy, T. E. Organization of Vomeronasal Sensory Coding Revealed by Fast Volumetric Calcium Imaging. *Journal of Neuroscience* **32**, 1612-1621, doi:10.1523/JNEUROSCI.5339-11.2012 (2012).
- 12 Reddy, G. D., Kelleher, K., Fink, R. & Saggau, P. Three-dimensional random access multiphoton microscopy for functional imaging of neuronal activity. *Nat. Neurosci.* **11**, 713-720, doi:10.1038/nn.2116 (2008).
- 13 Salome, R. *et al.* Ultrafast random-access scanning in two-photon microscopy using acousto-optic deflectors. *J. Neurosci. Methods* **154**, 161-174, doi:10.1016/j.jnemeth.2005.12.010 (2006).
- 14 Katona, G. *et al.* Fast two-photon in vivo imaging with three-dimensional random-access scanning in large tissue volumes. *Nature methods* **9**, 201-208, doi:10.1038/nmeth.1851 (2012).
- 15 Grewe, B. F., Langer, D., Kasper, H., Kampa, B. M. & Helmchen, F. High-speed in vivo calcium imaging reveals neuronal network activity with near-millisecond precision. *Nature Methods* **7**, 399-U391 (2010).
- 16 Cheng, A., Goncalves, J. T., Golshani, P., Arisaka, K. & Portera-Cailliau, C. Simultaneous two-photon calcium imaging at different depths with

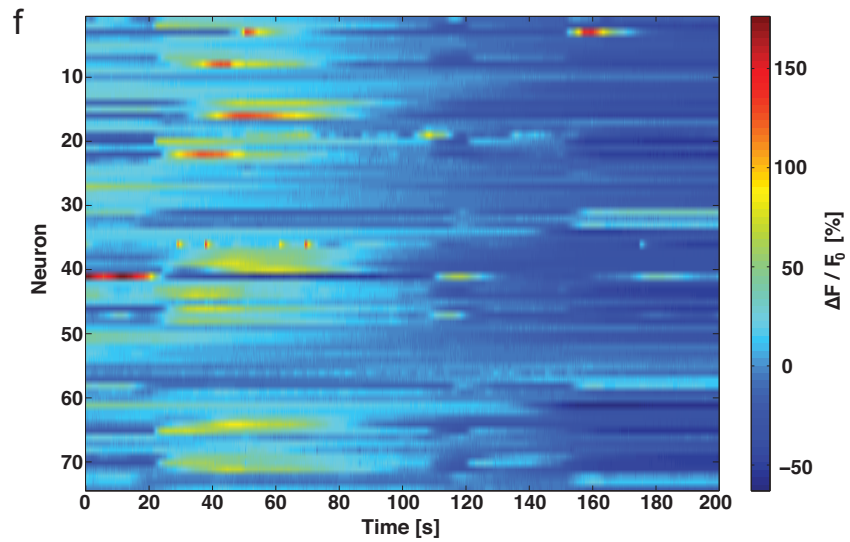
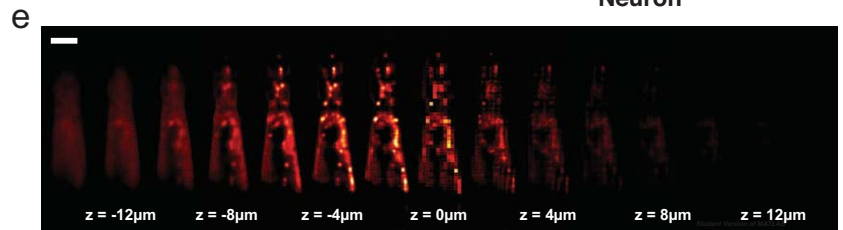
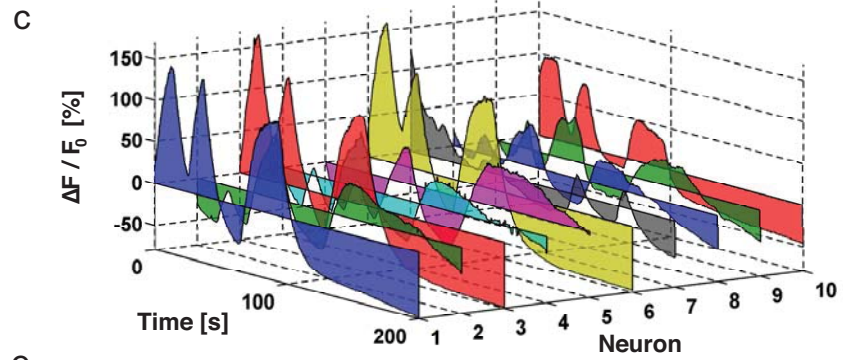
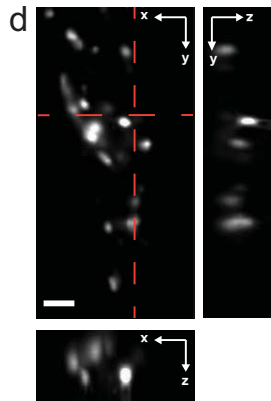
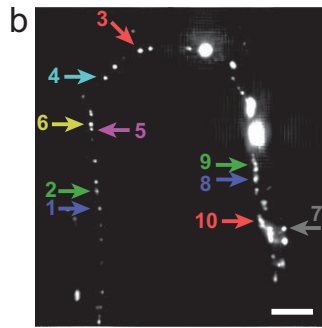
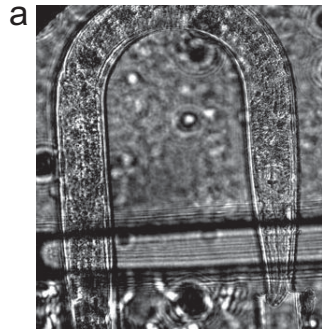
- spatiotemporal multiplexing. *Nature Methods* **8**, 139-U158, doi:10.1038/nmeth.1552 (2011).
- 17 Abrahamsson, S. *et al.* Fast multicolor 3D imaging using aberration-corrected multifocus microscopy. *Nature Methods* **10**, 60-U80, doi:10.1038/nmeth.2277 (2013).
- 18 Fenimore, E. E. & Cannon, T. M. CODED APERTURE IMAGING WITH UNIFORMLY REDUNDANT ARRAYS. *Appl. Optics* **17**, 337-347, doi:10.1364/ao.17.000337 (1978).
- 19 Zhou, C. Y., Lin, S., Nayar, S. & Ieee. in *2009 Ieee 12th International Conference on Computer Vision IEEE International Conference on Computer Vision* 325-332 (Ieee, 2009).
- 20 Bando, Y., Chen, B. Y. & Nishita, T. Extracting Depth and Matte using a Color-Filtered Aperture. *ACM Trans. Graph.* **27**, 9, doi:134 10.1145/1409060.1409087 (2008).
- 21 Llull, P. *et al.* Coded aperture compressive temporal imaging. *Optics Express* **21**, 10526-10545, doi:10.1364/oe.21.010526 (2013).
- 22 Horisaki, R., Irie, S., Ogura, Y. & Tanida, J. Three-dimensional information acquisition using a compound imaging system. *Opt. Rev.* **14**, 347-350, doi:10.1007/s10043-007-0347-z (2007).
- 23 Isaksen, A., McMillan, L., Gortler, S. J. & Acm. in *Siggraph 2000 Conference Proceedings Computer Graphics* 297-306 (Assoc Computing Machinery, 2000).
- 24 Ng, R. Fourier slice photography. *ACM Trans. Graph.* **24**, 735-744, doi:10.1145/1073204.1073256 (2005).
- 25 Levoy, M., Ng, R., Adams, A., Footer, M. & Horowitz, M. Light field microscopy. *ACM Trans. Graph.* **25**, 924-934, doi:10.1145/1141911.1141976 (2006).
- 26 Levoy, M., Zhang, Z. & McDowall, I. Recording and controlling the 4D light field in a microscope using microlens arrays. *J. Microsc.* **235**, 144-162 (2009).
- 27 Levoy, M. *et al.* Synthetic aperture confocal imaging. *ACM Trans. Graph.* **23**, 825-834, doi:10.1145/1015706.1015806 (2004).
- 28 Horisaki, R., Xiao, X., Tanida, J. & Javidi, B. Feasibility study for compressive multi-dimensional integral imaging. *Optics Express* **21**, 4263-4279 (2013).
- 29 Pipponnier, M. *et al.* Three-dimensional imaging using continuously self-imaging gratings. *Opt. Lett.* **38**, 4058-4061, doi:10.1364/ol.38.004058 (2013).
- 30 Quirin, S., Peterka, D. S. & Yuste, R. Instantaneous three-dimensional sensing using spatial light modulator illumination with extended depth of field imaging. *Optics Express* **21**, 16007-16021, doi:10.1364/oe.21.016007 (2013).
- 31 Agard, D. A. OPTICAL SECTIONING MICROSCOPY - CELLULAR ARCHITECTURE IN 3 DIMENSIONS. *Annual Review of Biophysics and Bioengineering* **13**, 191-219 (1984).
- 32 Broxton, M. *et al.* Wave optics theory and 3-D deconvolution for the light field microscope. *Optics Express* **21**, 25418-25439, doi:10.1364/oe.21.025418 (2013).

- 33 Vogelstein, J. T. *et al.* Spike Inference from Calcium Imaging Using Sequential Monte Carlo Methods. *Biophys. J.* **97**, 636-655, doi:10.1016/j.bpj.2008.08.005 (2009).
- 34 Mukamel, E. A., Nimmerjahn, A. & Schnitzer, M. J. Automated Analysis of Cellular Signals from Large-Scale Calcium Imaging Data. *Neuron* **63**, 747-760, doi:10.1016/j.neuron.2009.08.009 (2009).
- 35 Faumont, S. *et al.* An Image-Free Opto-Mechanical System for Creating Virtual Environments and Imaging Neuronal Activity in Freely Moving *Caenorhabditis elegans*. *PLoS One* **6**, 12, doi:e24666 10.1371/journal.pone.0024666 (2011).
- 36 Ohkura, M., Sasaki, T., Kobayashi, C., Ikegaya, Y. & Nakai, J. An Improved Genetically Encoded Red Fluorescent Ca<sup>2+</sup> Indicator for Detecting Optically Evoked Action Potentials. *PLoS One* **7**, 7, doi:e39933 10.1371/journal.pone.0039933 (2012).
- 37 Akerboom, J. *et al.* Genetically encoded calcium indicators for multi-color neural activity imaging and combination with optogenetics. *Frontiers in Molecular Neuroscience* **6**, doi:10.3389/fnmol.2013.00002 (2013).
- 38 Wu, J. H. *et al.* Improved Orange and Red Ca<sup>2+</sup> Indicators and Photophysical Considerations for Optogenetic Applications. *ACS Chem. Neurosci.* **4**, 963-972, doi:10.1021/cn400012b (2013).
- 39 Booth, M. J. Adaptive optics in microscopy. *Philos. Trans. R. Soc. A-Math. Phys. Eng. Sci.* **365**, 2829-2843, doi:10.1098/rsta.2007.0013 (2007).
- 40 Ntziachristos, V. Going deeper than microscopy: the optical imaging frontier in biology. *Nature Methods* **7**, 603-614, doi:10.1038/nmeth.1483 (2010).
- 41 Kak, A. C. & Slaney, M. Principles of Computerized Tomographic Imaging. *Classics in Applied Mathematics* ISBN: 978-0-89871-494-4 (2001).
- 42 Gu, M. Advanced Optical Imaging Theory Springer ISBN-10: 981402130X (1999).

Figure 1: Light field deconvolution microscopy (LFDM). (a) A microlens array is appended to the camera port of a standard wide-field microscope. The lens array (pitch  $150\mu\text{m}$ , focal length  $3\text{mm}$ , OKO Tech) is placed in the primary image plane of the fluorescence microscope. The array itself is imaged with a 1:1 relay lens system onto the chip of a sCMOS camera. See Methods for details. The inset shows a close-up picture of the microlens array. (b) The point spread function (PSF) of a sub-diffraction sized bead located at  $z=7.5\mu\text{m}$  off the focal plane, as seen through the microlens array. Scale bar  $150\mu\text{m}$  in (a-b). c) Axial ( $xz$ ) PSF at  $z=7.5\mu\text{m}$ , reconstructed using LFDM, and corresponding  $x$ - as well as  $z$ -profiles, showing lateral and axial resolution, respectively. Scale bar  $3\mu\text{m}$ . (d) Maximum-intensity projection of a deconvolved wide-field focal stack taken without microlenses. The sample consists of  $6\mu\text{m}$ -sized fluorescent beads in agarose, mimicking the distribution of neurons in *C. elegans*. (e) Zoom-in of highlighted area, with  $xz$ - as well as  $yz$ -section maximum-intensity projections. The individual beads are well resolved in this image. (e,f) Corresponding volume of the same beads,  $4\text{-}28\mu\text{m}$  off the focal plane, reconstructed via 15 iterations of light field deconvolution algorithm. Although the fluorescence of some lower lying beads is faintly visible, individual beads can still be well resolved. Scale bar  $10\mu\text{m}$  in (d-g).

Figure 2: Whole animal  $\text{Ca}^{2+}$ -imaging of *Caenorhabditis elegans* using light field microscopy. (a) Wide-field image of the worm inside a microfluidic poly(dimethylsiloxane) (PDMS) device used to immobilise the worm. Head is at bottom right. (b) Maximum intensity projection (MIP) of light field deconvolved image (15 iterations) containing 14 distinct z planes. The majority of the worm and its nervous system are clearly visible, including the head ganglia (at bottom right) as well as the ventral cord. Scale bar  $50\mu\text{m}$ . (c)  $\text{Ca}^{2+}$ -intensity traces ( $\Delta F/F_0$ ) of NLS-GCaMP5K fluorescence of selected neurons in the ventral cord and head region, as indicated by colored arrows and numbers in (b), and imaged volumetrically at 5 Hz for 200 seconds. Also see Supplementary Video 1. (d) Zoom of the brain region, with MIP of  $xy$  plane as well as  $xz$  and  $yz$  cross-sections indicated by the dashed lines. Single neurons are well resolved. Scale bar  $10\mu\text{m}$ . See also Supplementary Figure S1 and Supplementary Video 2. (e) Individual z planes of typical recording of the worm's brain, reconstructed from a single camera exposure (for higher resolution figure and neuron IDs, see Supplementary Fig. S2). In this recording, the worm's center was placed at the focal plane of the objective. Scale bar  $50\mu\text{m}$ . (f) Activity of all 74 neurons identified in (e), also see Supplementary Video 4. Each row shows a time-series heat map. Color indicates percent fluorescence changes ( $\Delta F/F_0$ ); scaling is indicated by the color bar on the right. The x-axis in (f) represents elapsed recording time while the y axis shows individual neurons (see Supplementary Fig. S2 for neuron IDs).





## Supplementary Information

### Simultaneous whole-animal 3D-imaging of neuronal activity using light field microscopy

Robert Prevedel<sup>1-3,\*</sup>, Young-Gyu Yoon<sup>4,5,\*</sup>, Maximilian Hoffmann<sup>1-3</sup>, Nikita Pak<sup>5,6</sup>, Gordon Wetzstein<sup>5</sup>, Saul Kato<sup>1</sup>, Tina Schrödel<sup>1</sup>, Ramesh Raskar<sup>5</sup>, Manuel Zimmer<sup>1</sup>, Edward S. Boyden<sup>5,7,8</sup>, Alipasha Vaziri<sup>1-3</sup>

<sup>1</sup>Research Institute of Molecular Pathology, Vienna, Austria.

<sup>2</sup>Max F. Perutz Laboratories, University of Vienna, Vienna, Austria.

<sup>3</sup>Research Platform Quantum Phenomena & Nanoscale Biological Systems (QuNaBioS), University of Vienna, Vienna, Austria.

<sup>4</sup>Department of Electrical Engineering and Computer Science, Massachusetts Institute of Technology (MIT), Cambridge, MA, USA

<sup>5</sup>MIT Media Lab, Massachusetts Institute of Technology (MIT), Cambridge, MA, USA

<sup>6</sup>Department of Mechanical Engineering, Massachusetts Institute of Technology (MIT), Cambridge, MA, USA

<sup>7</sup>Departments of Biological Engineering and Brain and Cognitive Sciences, Massachusetts Institute of Technology (MIT), Cambridge, MA, USA

<sup>8</sup>McGovern Institute, Massachusetts Institute of Technology (MIT), Cambridge, MA, USA

\* These authors contributed equally to this work.

Correspondence should be addressed to E.S.B. ([esb@media.mit.edu](mailto:esb@media.mit.edu)) or A.V. ([vaziri@imp.ac.at](mailto:vaziri@imp.ac.at)).

#### Supplementary Information

**Supplementary Note 1** Optical design choices and their effect on resolution in 3D deconvolution light field microscopy.

**Supplementary Note 2** Volume reconstruction for 3D-deconvolution light field microscopy and computing requirements.

#### Supplementary Figures

**Supplementary Figure S1.** Whole-animal Ca<sup>2+</sup>-imaging of *C. elegans*.

**Supplementary Figure S2.** High-resolution images of Fig. 2e and Fig. 2f indicating Neuron ID numbers in z-planes and heatmap map of neuronal activity of all neurons.

**Supplementary video legends.**

**Supplementary software description.**

## Supplementary Information

### Supplementary Note 1 Optical design choices and their effect on resolution in 3D deconvolution light field microscopy.

The choice of objective and microlens array determines the spatial resolution and field-of-view in all three dimensions. The pitch, i.e. the distance between the microlenses, in combination with the sensor's pixel size and objective magnification controls trade-off between spatial resolution vs. field-of-view while the objective's magnification and numerical aperture control axial resolution vs. axial range. Furthermore, the field-number of the microlenses needs to match that of the objective in order to preserve the maximum angular information in the light fields <sup>1</sup>.

Due to the variation in sampling density, reconstructed volumes have a lateral resolution that varies along the optical axis. On the focal plane, achievable resolution is equivalent to conventional LFM, i.e. the size of each microlens divided by the magnification of the objective lens ( $150\mu\text{m}/40\times = 3.75\mu\text{m}$  in our system). The resolution increases for lateral sections close to the focal plane,  $\sim 1.5\mu\text{m}$  laterally in our implementation, but drops at larger distances, e.g. to  $\sim 3\mu\text{m}$  laterally at  $-25\mu\text{m}$ , in accordance with Ref. <sup>2</sup>.

### Supplementary Note 2 Volume reconstruction for 3D-deconvolution light field microscopy and computing requirements.

The software for 3D reconstruction was written in MATLAB (Mathworks) using its parallel computing toolbox to enable multi-core processing. The software consists of three different parts: point spread function (PSF) computation, image rectification / calibration, and 3D volume reconstruction. To generate PSFs, we compute the wavefront imaged through the microlens array for multiple points in the volume <sup>3</sup>. In contrast to previously implemented methods <sup>2</sup>, here we calculate the PSF using vectorial diffraction theory instead of scalar diffraction theory which enables us to faithfully model high NA objective lenses. We also exploit the circular symmetric of PSF for its computation, which results in a boost in computational speed. To faithfully represent the high spatial frequency component of the wavefront, computations are performed with a spatial oversampling factor of 3x compared to the size of the sensor pixels.

For the image rectification and calibration, the size and location of each microlens with respect to the sensor pixels are estimated using calibration images showing a fluorescent slide and a collimated beam. Once the size and the location of each microlens is determined, captured images are resampled to contain 15x15 angular light field samples under each microlens. The target axial resolution of reconstructed volumes is 2  $\mu\text{m}$ , which requires 12-16 z-slices for worm samples.

Reconstructing individual frames of recorded image sequences using Richardson-Lucy deconvolution method took between 20 and 90 min, depending on the size of the cropped image, on a workstation using 12-cores of a Intel Xeon E2650 "Sandy Bridge" processor and 32GB of RAM. Specifically, the reconstruction of only the head ganglia region of *C. elegans* took about 20 minutes where the reconstruction of the whole *C. elegans* took about 90 minutes with 8 iterations of the deconvolution algorithm.

However, reconstruction times of image sequences could be further optimized by using the reconstructed volume of one frame as the initial guess for the next. This removes the need for multiple algorithmic iterations at each frame and is well-justified because the imaging speed was sufficiently faster than both neuronal activity and movement of the worm.

## References

- <sup>1</sup> Levoy, M., Ng, R., Adams, A., Footer, M. & Horowitz, M. Light field microscopy. *ACM Trans. Graph.* **25**, 924-934, doi:10.1145/1141911.1141976 (2006).
- <sup>2</sup> Broxton, M. *et al.* Wave optics theory and 3-D deconvolution for the light field microscope. *Optics Express* **21**, 25418-25439, doi:10.1364/oe.21.025418 (2013).
- <sup>3</sup> Gu, M. *Advanced Optical Imaging Theory Springer ISBN-10: 981402130X* (1999).

## Supplementary Figures

### **Supplementary Figure S1.** Whole-animal Ca<sup>2+</sup>-imaging of *C. elegans*.

(a) Maximum intensity projection (MIP) of lightfield deconvolved image (15 iterations) of the whole worm shown in Fig. 2d, containing 14 distinct z planes. Neurons contained in red boxes were further analyzed in (b-f). NeuronIDs of z-stack in (b) match with heatplot map of neuronal activity in (f) and show neurons identified in the head using an automated segmentation algorithm, while (c) shows neuronIDs along the ventral cord with corresponding heatplot map shown in (e). Scale bar 50um.

**Supplementary Figure S2.** High-resolution images of Fig. 2e and Fig. 2f indicating Neuron ID numbers in z-planes in (a) and heatplot map of neuronal activity of all neurons in (b).

## **Supplementary video legends.**

### **Supplementary Video 1. Whole animal Ca<sup>2+</sup>-imaging of *C. elegans***

Maximum intensity projection of 14 z-planes at 2 $\mu$ m distance of a *Punc-31::NLS-GCaMP5K* worm. Shown are 200 seconds of recording of basal activity at 5Hz volume rate (1000 frames in total). Video frame rate is 100 frames per second, which equates to 20 seconds in real time in the video (i.e. playback speed 20x). See also Figure 2a-c.

### **Supplementary Video 2. Whole animal Ca<sup>2+</sup>-imaging of *C. elegans***

Maximum intensity projection of 14 z-planes at 2 $\mu$ m distance of a *Punc-31::NLS-GCaMP5K* worm. Shown are 200 seconds of recording of basal activity at 5Hz volume rate. Video frame rate is 100 frames per second, which equates to 20 seconds in real time in the video (i.e. playback speed 20x). See also Figure 2d.

### **Supplementary Video 3. High-speed brain-wide Ca<sup>2+</sup>-imaging of *C. elegans* at 50Hz**

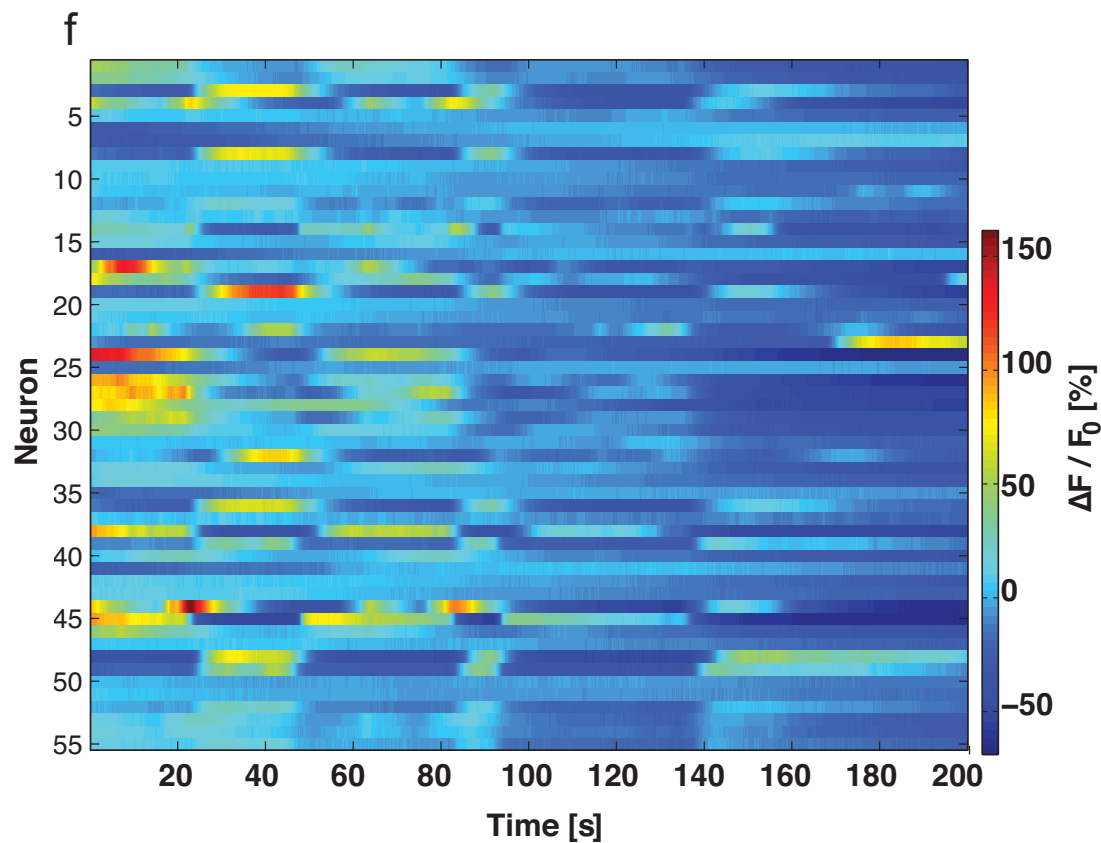
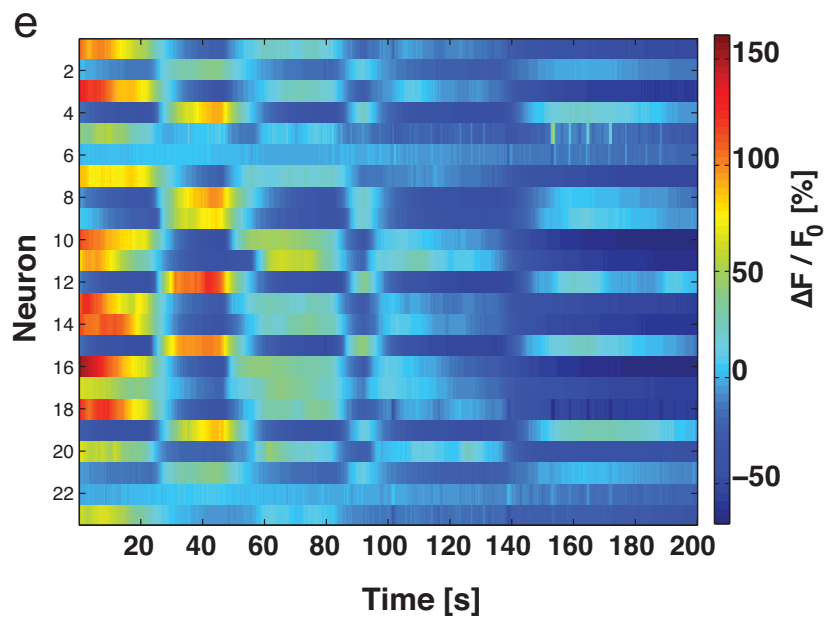
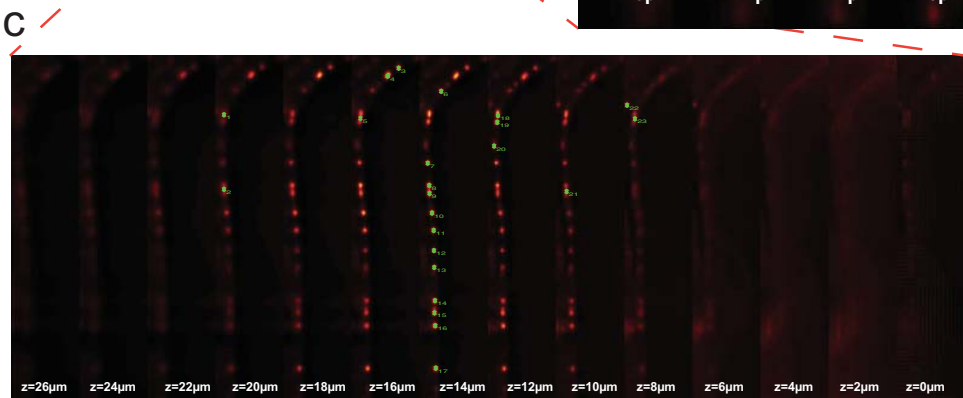
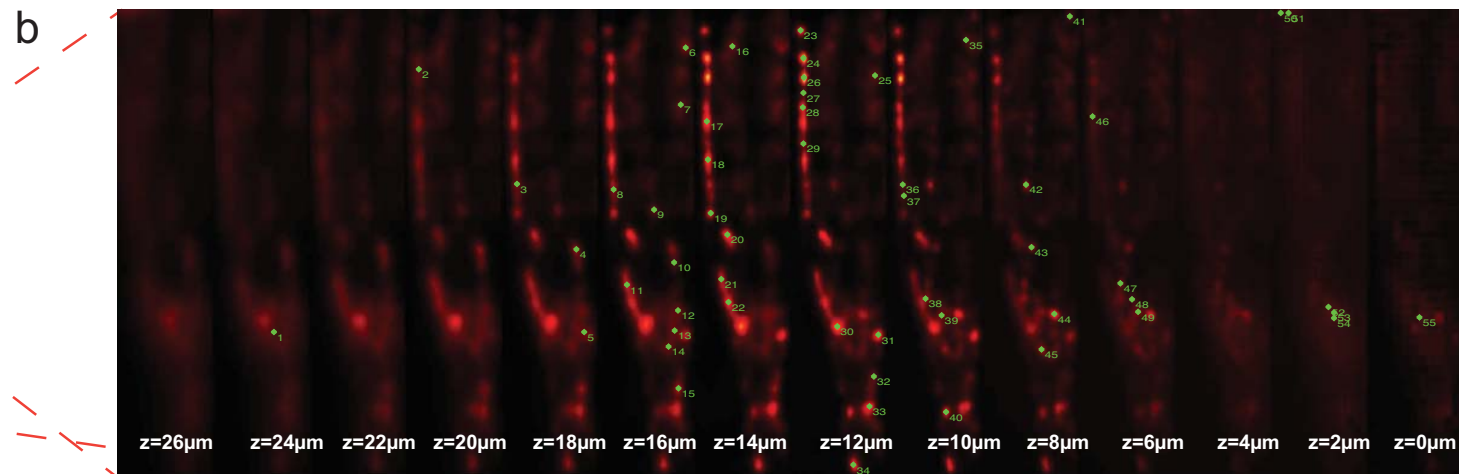
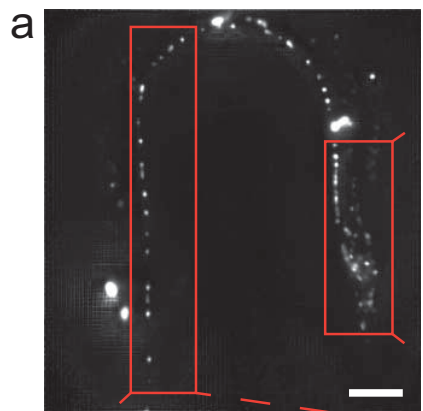
Maximum intensity projection of 12 z-planes at 2 $\mu$ m distance of a *Punc-31::NLS-GCaMP5K* worm. Shown are 40 seconds of recording of basal activity in the head ganglia at 50Hz volume rate. Exposure time for individual volumes was 13ms, and excitation power was 25mW, provided by a 488nm laser. Video frame rate is 500 frames per second, which equates to 500 volumes per second in the video (i.e. playback speed 10x).

### **Supplementary Video 4. Brain-wide Ca<sup>2+</sup>-imaging of *C. elegans***

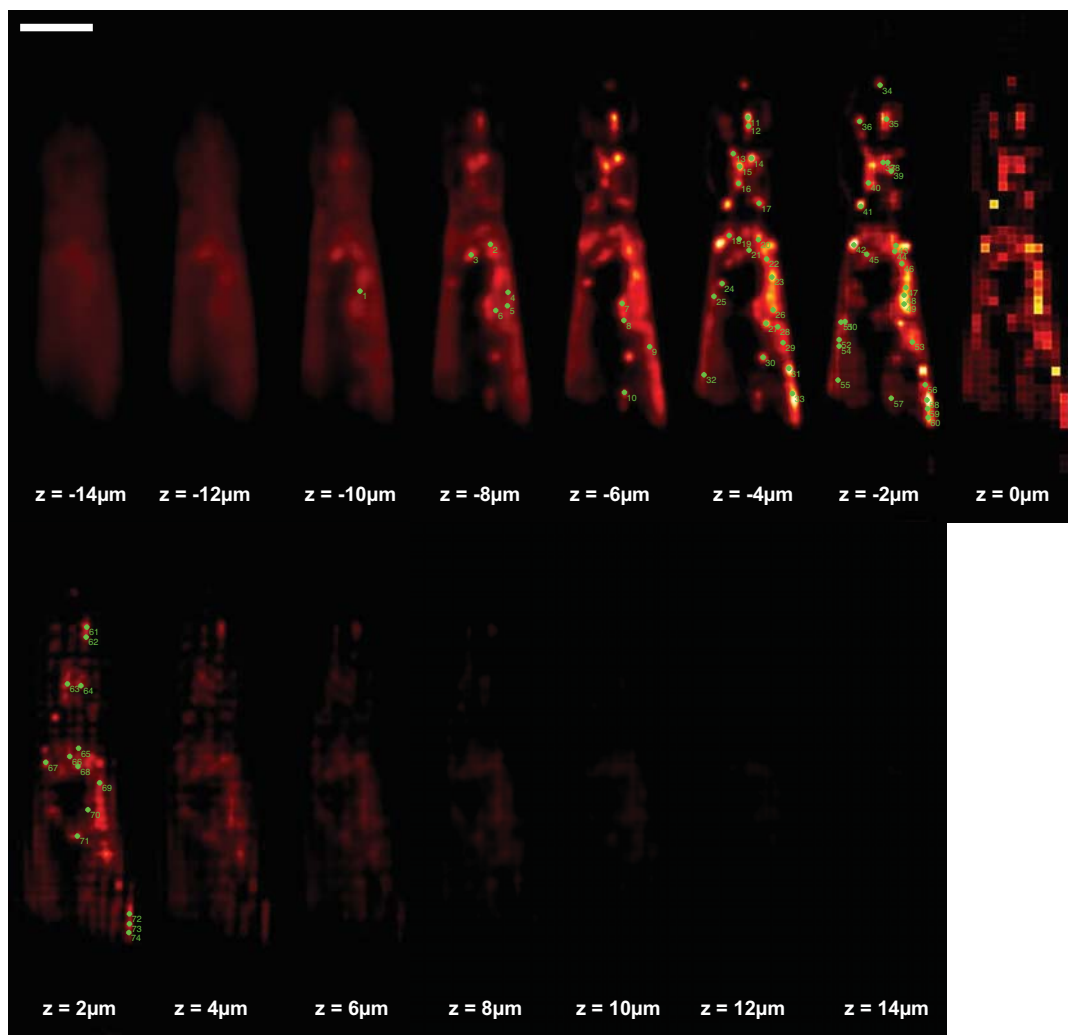
Maximum intensity projection of 15 z-planes at 2 $\mu$ m distance of a *Punc-31::NLS-GCaMP5K* worm. Shown are 200 seconds of recording of basal activity in the head ganglia at 5Hz volume rate. Video frame rate is 100 frames per second, which equates to 20 seconds in real time in the video (i.e. playback speed 20x). See also Figure 2e-f.

## **Supplementary software description.**

The software for 3D volume reconstruction from light-field images is available as Supplementary Software 1. It was written in MATLAB. As a preprocessing step, PSF computing function (computePSF.m) and image rectifying function ImageRectification.m) need to be run prior to running reconstruction function (Reconstruction3D.m). It also includes sample raw images of *C. elegans*' head ganglia region for testing. It requires MATLAB2013a and we recommend workstations with 12-core Intel Xeon processor and at least 32GB of RAM.



a



b

